

**Observation of three-mode parametric interactions in long optical cavities**C. Zhao,<sup>\*</sup> L. Ju, Y. Fan, S. Gras, B. J. J. Slagmolen,<sup>†</sup> H. Miao, P. Barriga, and D. G. Blair  
*School of Physics, University of Western Australia, 35 Stirling Highway, Crawley, Western Australia 6009, Australia*D. J. Hosken, A. F. Brooks,<sup>‡</sup> P. J. Veitch, D. Mudge, and J. Munch  
*Department of Physics, The University of Adelaide, Adelaide, South Australia, 5005 Australia*

(Received 17 December 2007; published 6 August 2008)

We report the observation of three-mode optoacoustic parametric interactions of the type predicted to cause parametric instabilities in a 77-m-long, high-optical-power cavity that uses suspended sapphire mirrors. Resonant interaction occurs between two distinct optical modes and an acoustic mode of one mirror when the difference in frequency between the two optical cavity modes is close to the frequency of the acoustic mode. Experimental results validate the theory of parametric instability in high-power optical cavities, and demonstrate tunable parametric gain  $\sim 10^{-2}$  and more than 20 dB amplification of a high-order optical mode power generated by an applied acoustic signal.

DOI: [10.1103/PhysRevA.78.023807](https://doi.org/10.1103/PhysRevA.78.023807)

PACS number(s): 42.65.Yj, 04.80.Nn, 42.79.Gn, 42.79.Jq

**I. INTRODUCTION**

The principles of parametric interactions have been widely used in physics, including low-noise microwave amplifiers, optical parametric amplifiers (OPAs), and optical spring interactions with mechanical resonators. In the case of optomechanical interactions a mechanical mode modulates the length of an optical cavity, thereby changing the resonance condition of the optical mode. Such interactions have been observed in [1–3] and have recently been used to “cool” thermally excited mechanical modes of small acoustic resonators through the associated time-dependent radiation pressure forces acting on the resonator [4–8]. Such techniques are examples of two-mode parametric interactions in which the linewidth of the optical mode is sufficiently broad that the mechanical frequency occurs within the linewidth of a single mode. The phenomenon reported here is analogous to stimulated Brillouin scattering (SBS) [9,10]. In this case an optical mode from a resonator excites an acoustic hypersonic wave in a material at optical wavelengths, from which a second optical mode in the same resonator is excited by scattering off the moving sound grating. Three-mode scattering into symmetric cavity longitudinal modes has been studied in a laser interferometer gravitational-wave observatory (LIGO) interferometer [11]. To cause parametric instabilities the scattering must occur into cavity modes which are distributed asymmetrically (in frequency space) about the carrier frequency. In addition, the transverse structure of the optical mode must match an acoustic mode structure.

Here we present the observation of such three-mode optoacoustic parametric interactions. In this case a cavity fundamental mode and a first-order transverse mode interact with a low-frequency acoustic mode of a mirror. The energy

in the cavity fundamental mode (carrier) is scattered into the first-order transverse mode (sideband) by its interaction with an acoustic mode in one of the cavity mirrors. In high-power and low-loss systems, this interaction can lead to parametric instability.

A one-dimensional analysis of three-mode optoacoustic parametric interactions in the context of advanced gravitational wave interferometers was described by Braginsky *et al.* [12,13]. Their analysis was extended by Zhao *et al.* [14] to include the three-dimensional (3D) acoustic mode structure of the mirrors and the optical cavity mode shapes. Ju *et al.* [15] went on to consider the effect of parametric scattering into multiple optical modes.

These analyses predict that many of the features that optimize the sensitivity of advanced gravitational wave detectors also increase the likelihood of the parametric excitation of its mirrors. In particular, the new generation of advanced interferometers will use large mirrors that have low acoustic losses to reduce the effects of radiation pressure fluctuations and Brownian noise, respectively. They use long optical cavities and extremely high stored power to reduce the effect of shot noise. The resulting high optical and acoustic mode densities plus high optical power, can lead to a risk of parametric excitation of the mirrors without careful design. It is therefore important that the above analyses be validated so that the practical importance of parametric instabilities can be assessed. Here we present experimental results for three-mode parametric interactions. Measurements are in agreement with the theory [12] and consistent with specific predictions for this experiment [16].

**II. THREE-MODE OPTOACOUSTIC PARAMETRIC INTERACTIONS**

Parametric interactions can be considered as simple scattering processes [17], as indicated in Fig. 1. In Fig. 1(a) a photon of frequency  $\omega_0$  is scattered, creating a lower-frequency (Stokes) photon of frequency  $\omega_s$  and a phonon of frequency  $\omega_m$ , which increases the occupation number of the acoustic mode. In Fig. 1(b) a photon of frequency  $\omega_0$  is scat-

<sup>\*</sup>zhao@physics.uwa.edu.au<sup>†</sup>Present address: Centre for Gravitational Physics, The Australian National University, Canberra, 0200, Australia<sup>‡</sup>Present address: LIGO, California Institute of Technology, Pasadena, CA, USA.

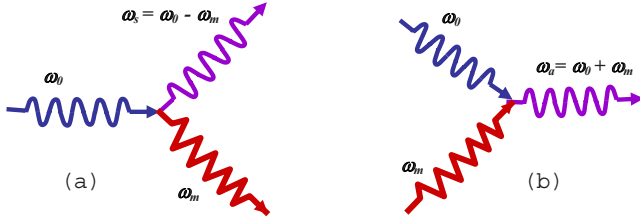


FIG. 1. (Color online) Parametric scattering of a photon of frequency  $\omega_0$  (a) into a lower-frequency Stokes photon  $\omega_s$  and a phonon  $\omega_m$ , and (b) into a higher-frequency anti-Stokes photon  $\omega_a$ , which require destruction of a phonon.

tered from a phonon, creating a higher-frequency (anti-Stokes) photon of frequency, which requires that the acoustic mode is a source of phonons, thus reducing its occupation number. The scattering could create entangled pairs of phonons and photons [18].

This three-mode interaction can occur strongly only if two conditions are met simultaneously. First, the optical cavity must support eigenmodes that have a frequency difference approximately equal to the acoustic frequency:  $|\omega_0 - \omega_{s(a)}| \approx \omega_m$ . Second, the optical and acoustic modes must have a suitable spatial overlap. The three-mode interaction in an optical cavity is shown schematically in Fig. 2, where we assume that only the end mirror is vibrating. The vibration of the end mirror surface scatters part of the cavity TEM<sub>00</sub> mode into two sidebands of frequencies higher or lower than the TEM<sub>00</sub> mode frequency by  $\omega_m$ , the acoustic mode frequency. Depending on the end mirror acoustic mode pattern on the mirror surface, the scattered sidebands may overlap with the cavity high-order modes. If the acoustic mode frequency is equal to the frequency difference between the TEM<sub>00</sub> mode and the cavity high-order modes, then one of the scattered sidebands may resonate inside the cavity. The interactions between TEM<sub>00</sub> mode and scattered light will create radiation pressure back action on the end mirror at the differential frequency ( $|\omega_0 - \omega_{s(a)}| = \omega_m$ ) between the TEM<sub>00</sub> mode and scattered light. If the lower sideband is resonant, the back action will excite the mirror acoustic mode and transfer the energy from light to the acoustic mode. If the higher sideband is resonant, the back action will damp the acoustic mode by transferring acoustic mode energy to the light. Only if the cavity had a pair of high-order modes spaced symmetrically on either side of the TEM<sub>00</sub> mode could both sidebands exist simultaneously. Then the excitation and damping effects will cancel each other. However, this is rare because of the asymmetric nature of the cavity mode structure.

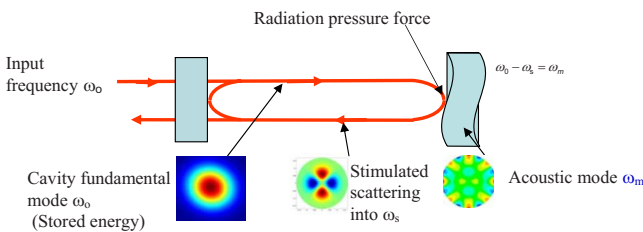


FIG. 2. (Color online) Schematic diagram of three-mode interactions in an optical cavity.

By solving the coupled dynamic equations of the acoustic mode and the cavity optical modes including radiation pressure back action described above, Braginsky *et al.* [13] obtained a dimensionless parametric gain  $R$ , given in Eq. (1), to characterize the effect of the parametric scattering. In general, there may be multiple Stokes (excitation) and anti-Stokes (damping) interactions for each acoustic mode. The positive  $R$  indicates that the interaction is dominated by excitation and negative  $R$  indicates that the interaction is dominated by damping. For simplicity, we include only one of each interaction type [13]:

$$\mathcal{R} = \frac{4PQ_m}{McL\omega_m^2} \left( \frac{Q_s\Lambda_s}{1 + (\Delta\omega_s/\gamma_s)^2} - \frac{Q_a\Lambda_a}{1 + (\Delta\omega_a/\gamma_a)^2} \right). \quad (1)$$

Here  $Q_m$  is the quality factor of the acoustic mode,  $M$  is the mass of the mechanical resonator,  $P$  is the power stored in the TEM<sub>00</sub> mode,  $L$  is the length of the cavity, and  $\Delta\omega_{s(a)} = |\omega_0 - \omega_{s(a)}| - \omega_m = \Delta_{s(a)} - \omega_m$ ,  $\omega_{s(a)}$ ,  $Q_{s(a)}$ , and  $\delta_{s(a)} = \omega_{s(a)}/2Q_{s(a)}$  are the frequencies,  $Q$  factors and linewidths of Stokes (anti-Stokes) optical modes.  $\Delta_{s(a)}$  is the difference between the TEM<sub>00</sub> mode and the higher-order Stokes (anti-Stokes) mode; and the overlap factors  $\Lambda_{s(a)}$  are given by [13]

$$\Lambda_{s(a)} = \frac{V \int |f_0(\vec{r}_\perp) f_{s(a)}(\vec{r}_\perp) u_z d\vec{r}_\perp|^2}{\int |f_0|^2 d\vec{r}_\perp \int |f_{s(a)}|^2 d\vec{r}_\perp \int |\vec{u}|^2 dV}, \quad (2)$$

where  $f_0$  and  $f_{s(a)}$  describe the optical field distribution over the mirror surface for the TEM<sub>00</sub> mode and higher-order modes, respectively,  $\vec{u}$  is the spatial displacement vector for the acoustic mode, and  $u_z$  is the component of  $\vec{u}$  normal to the mirror surface. The integrals  $\int d\vec{r}_\perp$  and  $\int dV$  correspond to integration over the mirror surface and the mirror volume  $V$ , respectively. The experiment described below investigated the scattering process between the TEM<sub>00</sub> mode and an anti-Stokes TEM<sub>01</sub> mode, so hereafter we omit the subscripts for  $\Delta\omega$ .

For positive  $R < 1$ , the amplitude of the acoustic mode is increased by a factor  $1/(1-R)$ . If  $R > 1$ , the amplitude should increase exponentially with time until non-linear losses lead to saturation. For negative values of  $R$ , energy is extracted from the acoustic mode and if it is normally in thermal equilibrium, the effective mode temperature is cooled to a value of  $\sim T/R$ , where  $T$  is the physical temperature of the acoustic resonator [6]. For  $R < 1$  the interaction also causes changes in the relaxation time of the acoustic mode.

The three-mode interaction could thus be observed by monitoring either the amplitude or relaxation time of the acoustic mode, or by measuring the amplitude of the anti-Stokes optical mode. In the experiment we report here, the maximum gain accessible was  $R \sim 10^{-2}$  and therefore we chose to measure the power scattered into an anti-Stokes TEM<sub>01</sub> mode of an optical cavity as the frequency difference  $\Delta\omega$  between the TEM<sub>00</sub> and TEM<sub>01</sub> modes was tuned across the 160 kHz acoustic resonance of a cavity mirror. The mirror was electrostatically excited using a comb capacitor [19] placed near the mirror's bottom back surface.

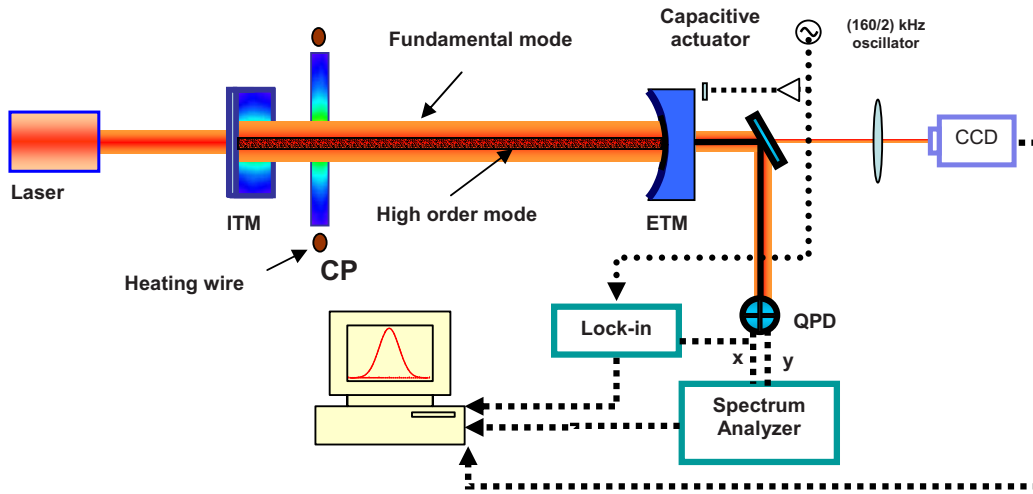


FIG. 3. (Color online) Schematic diagram of the measurement system. The single-frequency Nd:YAG laser was phase locked to a  $TEM_{00}$  mode of a 77-m suspended-mirror cavity. The end test mirror (ETM) was resonantly excited at the acoustic resonance. The fused silica compensation plate (CP) was heated around its cylindrical surface, thereby inducing a negative lens, which tuned the frequency difference between the  $TEM_{00}$  and  $TEM_{01}$  modes. The cavity tuning and the anti-Stokes  $TEM_{01}$  mode excitation were measured using the charge-coupled device (CCD) and quadrant photodiode (QPD) at the back of the ETM.

### III. EXPERIMENTAL OBSERVATION OF THREE-MODE PARAMETRIC INTERACTIONS

The layout of the measurement system is shown in Fig. 3. The optical cavity consists of two sapphire mirrors suspended 77 m apart on simple wire-loop pendula in a vacuum system, yielding a free-spectral range of about 1.9 MHz. The physical and optical parameters of the cavity are listed in Table I. The mirrors are aligned to produce a Fabry-Pérot cavity by applying magnetic forces to small magnets glued to the back of the mirrors [20].

The single-frequency neodymium-doped yttrium aluminum garnet (Nd:YAG) laser was phase locked and mode matched to the  $TEM_{00}$  mode of the optical cavity, providing about 4 W at the input test mirror (ITM). The  $TEM_{00}$  finesse of the optical cavity is  $1.3 \times 10^3$ , limited mostly by the absorption losses in the substrate of the rear-surface ITM, giving an intracavity  $TEM_{00}$  power of about 1 kW. The nominal cold-cavity beam radius at the end test mirror (ETM) is 9.2 mm, which is reduced by thermal lensing to 8.6 mm at full power.

The acoustic mode shape and hot-cavity overlap factor were calculated using finite-element modeling. The calcu-

lated contour map of the normal component at the ETM surface for the 158.11 kHz mode is shown in Fig. 4(a). The acoustic mode used for the measurement has a resonant frequency of 159.96 kHz, acceptably close to the calculated frequency, considering the magnets and suspension wire attached to the ETM, the accuracy of the material parameters, and numerical calculation accuracy [13]. The  $Q$  factor of this mode was measured to be  $Q \approx 7 \times 10^5$ . The overlap of this mode is indicated in Fig. 4(b), in which a vertical cross section of the product of the mode amplitude and the  $TEM_{00}$  mode is compared to the  $TEM_{01}$  mode amplitude. The overlap factor for this mode is 1.67, assuming that the optical mode is aligned with the geometric center of the ETM.

Tuning of the frequency of the  $TEM_{01}$  mode relative to that of the  $TEM_{00}$  mode was accomplished by using the intracavity low-absorption fused silica compensation plate shown in Fig. 3. Heating the CP around its cylindrical surface creates a negative thermal lens, thereby changing the  $g$  factor of the cavity, or, equivalently, the effective curvature of the ITM. The frequency difference between the  $TEM_{00}$  mode  $\omega_0$  and the anti-Stokes  $TEM_{01}$   $\omega_a$  is given by

TABLE I. Parameters of the cavity.

	ITM	ETM	CP
Radius of curvature (m)	Flat	720	Flat
Materials	Sapphire	Sapphire	Fused silica
Diameter (mm)	100	150	160
Thickness (mm)	46	80	17
High reflection (HR) coating transmission (ppm)	$1840 \pm 100$	20	
Anti-reflection (AR) coating reflectivity (ppm)	$29 \pm 20$	$12 \pm 12$	100
Cavity internal power (kW)	1		
Cavity length (m)	77		

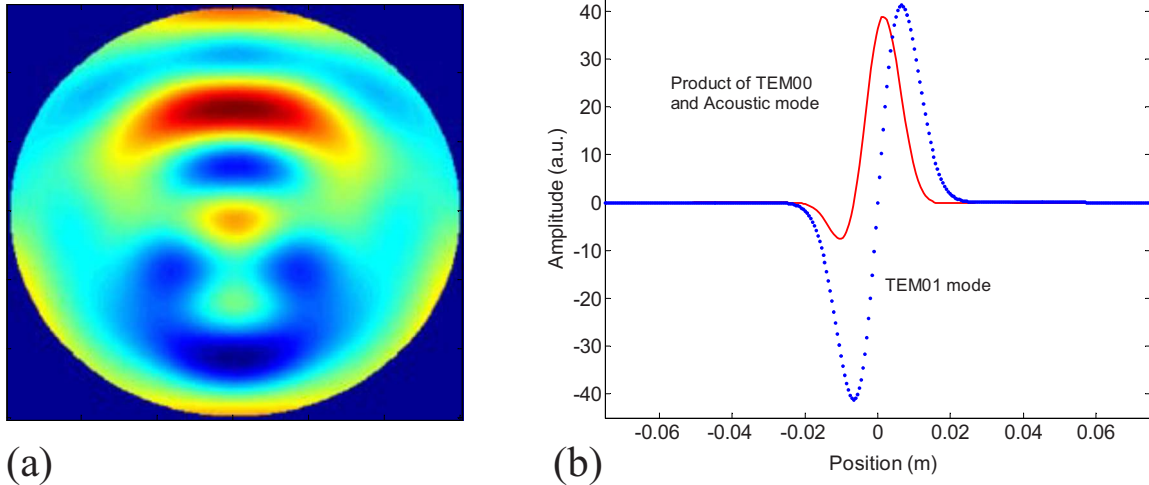


FIG. 4. (Color online) (a) A contour map of the normal component at the ETM surface of the acoustic mode at 158.11 kHz; (b) a vertical cross section of the product of the mode amplitude and the TEM<sub>00</sub> mode is compared to the TEM<sub>01</sub> mode amplitude.

$$\Delta\omega = \omega_0 - \omega_a = \frac{c}{L} \left[ \arccos \sqrt{\left(1 - \frac{L}{R_1}\right) \left(1 - \frac{L}{R_2}\right)} \right], \quad (3)$$

where  $R_1$  is the effective radius of curvature of the ITM and  $R_2$  is the radius of curvature of the ETM. Heating the CP with  $\sim 15$  W power over about 2 h increased the  $g$  factor from its nominal hot-cavity value of 0.87 to greater than 0.99.

The tuning of the cavity and the power in the TEM<sub>01</sub> mode were measured using the optical power leaking through the ETM. Some of this power was focused by a lens to create an image of the ETM spot onto a CCD camera. The spot size was used to calculate the effective curvature of the ITM and thus the frequency difference between the TEM<sub>00</sub> and TEM<sub>01</sub> modes.

The power in the TEM<sub>01</sub> mode was determined by using a differential readout of the quadrant photodiode to measure the heterodyne beat between the overlapping TEM<sub>00</sub> and TEM<sub>01</sub> modes. The differential readout discriminates against spurious signals due, for example, to direct acoustic modulation of the TEM<sub>00</sub> mode or electromagnetic pickup. Note that any spurious signals should be largely independent of the thermal tuning of the CP.

The square of the QPD voltage component at the acoustic mode frequency, which is proportional to power in the TEM<sub>01</sub> mode, is plotted as a function of the frequency difference between the TEM<sub>00</sub> and TEM<sub>01</sub> modes,  $\Delta\omega$ , in Fig. 5. Figure 5 also shows the parametric gain predicted by Eq. (1), using the measured input power, calculated overlap parameter, measured  $Q$  factors, and TEM<sub>01</sub> mode linewidth that was independently measured to be 1.46 kHz. The noise in the measured data is due to fluctuations in the cavity alignment, which affects the circulating power, the mode overlap, and the beam spot size measurement from which the mode spacing is inferred. The optical readout of the beat signal represents a direct measure of the transferred power. The energy transfer from the fundamental mode ranges from  $10^{-9}$  to  $10^{-7}$  of the TEM<sub>00</sub> mode power which is not detectable as

power loss in the TEM<sub>00</sub> mode. We can also see in Fig. 5 more than 20 dB amplification of the TEM<sub>01</sub> mode power generated by an applied acoustic signal.

We observed similar resonant parametric gain for another acoustic mode at  $\sim 84$  kHz. For this mode and the 160 kHz mode, we confirmed the linearity of the readout by observing an accurate exponential decay of the mirror mode using cavity readout. For the 84 kHz mode we also used an independent stress birefringence readout [21] of the acoustic mode to verify that the high-order mode signal is a true readout of the

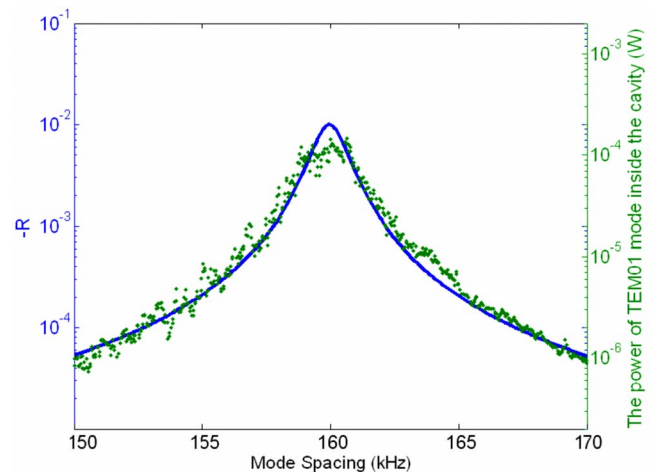


FIG. 5. (Color online) Measured power of the TEM<sub>01</sub> mode (dots) as a function of the frequency difference between the TEM<sub>00</sub> and TEM<sub>01</sub> modes (mode spacing). The peak power occurs at the frequency difference corresponding to a cavity  $g$  factor of 0.967. The solid line is the parametric gain predicted by Eq. (1), using the calculated overlap factor, the independently measured linewidth of both optical modes, the input power, and the measured acoustic mode  $Q$  factor. The relative scale of the two y axes has been corrected by a multiplicative parameter due to the uncertainty of the acoustic excitation amplitude. Measurement errors, predominantly due to alignment fluctuations, are worse at smaller mode spacing where the cavity  $g$  factor is higher.

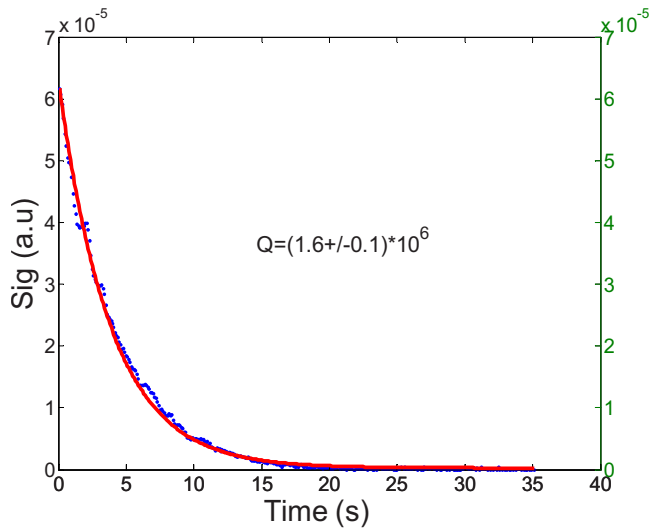


FIG. 6. (Color online) Recorded time trace of the QPD output demodulated at the 84 kHz acoustic mode frequency (dots) after the electrostatic excitation was stopped at time zero. The solid curve shows the expected exponential decay for the 84 kHz acoustic mode which had a  $Q$  factor of  $\sim 1.6 \times 10^6$ .

acoustic mode. Figure 6 shows the time trace for one of these measurements.

The magnitude of  $R$  is proportional to a product of three quality factors since the circulating power  $P$  scales with the  $\text{TEM}_{00}$  cavity loss. Our system has mirror  $Q$  factors limited by glued-on magnets, and optical losses limited by absorption in the internal substrate of the ITM and Fresnel reflection at the compensation plate. Nevertheless, we are able to observe the three-mode parametric interaction enhanced by the cavity resonance. The corresponding parametric gain as shown in Fig. 5 is  $\sim 0.01$ . This is insufficient to substantially change the acoustic mode relaxation time. However  $R \sim 100$  could be achieved by using cavity finesses  $\sim 10^4$ ,

acoustic mode  $Q_m \sim 4 \times 10^7$ , and a laser power of 20 W. For a Stokes mode, this gain would represent a severe parametric instability.

#### IV. CONCLUSIONS

We have observed a three-mode parametric interaction in a long optical cavity in which photons in a  $\text{TEM}_{00}$  optical mode are scattered by resonant acoustic phonons into a  $\text{TEM}_{01}$  mode. The system is analogous to SBS and also to an optical parametric amplifier except that one optical mode is replaced with an acoustic mode and the nonlinear interaction is via radiation pressure. We describe the system as an optoacoustic parametric amplifier (OAPA). By direct comparison with the OPA, the OAPA could be a source of phonon-photon entanglement and could find applications in quantum information, teleportation, and quantum encryption [18]. Much effort has already gone into defining methods for suppressing parametric instability in advanced gravitational wave detectors. A combination of low-noise damping rings [22] and stable power-recycling cavity design [23] is likely to lead to stable solutions.

#### ACKNOWLEDGMENTS

This investigation was conducted at the High Optical Power Facility, located at Gingin in Western Australia [24], which was developed in a collaboration between the Australian Consortium for Gravitational Astronomy and the U.S. LIGO Laboratory. We would like to thank the International Advisory Committee of the Gingin Facility for their encouragement and advice, and the Centre of Gravitational Physics of Australian National University for useful discussions and for providing cavity-locking electronics. This research was supported by the Australian Research Council and the Department of Education, Science and Training and by the U.S. National Science Foundation.

- 
- [1] T. Corbitt, Y. Chen, F. Khalili, D. Ottaway, S. Vyatchanin, S. Whitcomb, and N. Mavalvala, *Phys. Rev. A* **73**, 023801 (2006).
  - [2] T. J. Kippenberg, H. Rokhsari, T. Carmon, A. Scherer, and K. J. Vahala, *Phys. Rev. Lett.* **95**, 033901 (2005).
  - [3] B. S. Sheard, M. B. Gray, C. M. Mow-Lowry, D. E. McClelland, and S. E. Whitcomb, *Phys. Rev. A* **69**, 051801(R) (2004).
  - [4] S. Gigan, H. R. Böhm, M. Paternostro, F. Blaser, G. Langer, J. B. Hertzberg, K. C. Schwab, D. Bäuerle, M. Aspelmeyer, and A. Zeilinger, *Nature (London)* **444**, 67 (2006).
  - [5] A. Schliesser, P. DelHaye, N. Nooshi, K. J. Vahala, and T. J. Kippenberg, *Phys. Rev. Lett.* **97**, 243905 (2006).
  - [6] O. Arcizet, P. F. Cohandon, T. Briant, M. Pinard, and A. Heidmann, *Nature (London)* **444**, 71 (2006).
  - [7] T. Corbitt, Y. Chen, E. Innerhofer, H. Müller-Ebhardt, D. Ottaway, H. Rehbein, D. Sigg, S. Whitcomb, C. Wipf, and N. Mavalvala, *Phys. Rev. Lett.* **98**, 150802 (2007).
  - [8] C. M. Mow-Lowry, A. J. Mullavey, S. Goszler, M. B. Gray, and D. E. McClelland, *Phys. Rev. Lett.* **100**, 010801 (2008).
  - [9] H.-J. Eichler, R. Menzel, and D. Schumann, *Appl. Opt.* **31**, 5038 (1992).
  - [10] I. Yu. Anikeev and J. Munch, *Opt. Quantum Electron.* **31**, 545 (1999).
  - [11] W. E. Butler, Ph.D. thesis, University of Rochester, 2004.
  - [12] V. B. Braginsky, S. E. Strigin, and S. P. Vyatchanin, *Phys. Lett. A* **287**, 331 (2001).
  - [13] V. B. Braginsky and S. P. Vyatchanin, *Phys. Lett. A* **293**, 228 (2002).
  - [14] C. Zhao, L. Ju, J. Degallaix, S. Gras, and D. G. Blair, *Phys. Rev. Lett.* **94**, 121102 (2005).
  - [15] L. Ju, S. Gras, C. Zhao, J. Degallaix, and D. G. Blair, *Phys. Lett. A* **354**, 360 (2006).
  - [16] C. Zhao *et al.*, *J. Phys.: Conf. Ser.* **32**, 368 (2006).
  - [17] J. M. Manley and H. E. Row, *Proc. IRE* **44**, 904 (1956).
  - [18] S. Pirandola, S. Mancini, D. Vitali, and P. Tombesi, *Phys. Rev. A* **68**, 062317 (2003).
  - [19] A. Cadez and A. Abramovici, *J. Phys. E* **21**, 453 (1988).

- [20] LIGO Scientific Collaboration, B. Abbott *et al.*, Nucl. Instrum. Methods Phys. Res. A **517**, 154 (2004).
- [21] M. A. Beilby and P. R. Saulson, Rev. Sci. Instrum. **69**, 2539 (1998).
- [22] S. Gras, D. G. Blair, and L. Ju, Phys. Lett. A **372**, 1348 (2008).
- [23] G. Mueller (unpublished).
- [24] L. Ju *et al.*, Class. Quantum Grav. **21**, S887 (2004).